Phase synchronization inside a superradiant laser

Joshua M. Weiner, Kevin C. Cox, Justin G. Bohnet, and James K. Thompson

Phys. Rev. A **95**, 033808 — Published 9 March 2017

DOI: 10.1103/PhysRevA.95.033808

Phase Synchronization Inside a Superradiant Laser

Joshua M. Weiner, Kevin C. Cox, Justin G. Bohnet, and James K. Thompson
*JILA, NIST and Department of Physics, University of Colorado, Boulder, Colorado 80309-0440, USA**

Superradiant lasers may soon achieve state-of-the-art frequency purity, with linewidths of one milliHertz or less. In a superradiant, or bad-cavity laser, coherence is primarily stored in the atomic gain medium instead of the optical field. This phase storage is characterized by spontaneous quantum synchronization of the optical dipole moments of each atom. To observe this synchronization, we create two independent superradiant atomic ensembles lasing in a single optical cavity, observing the dynamics of phase re-alignment, collective power enhancement, and steady state frequency locking. This work introduces superradiant ensembles as a testbed for fundamental study of quantum synchronization as well and informs research on narrow linewdith superradiant lasers.

PACS numbers: 42.55.Ye, 32.80.Qk, 37.30.+i, 42.50.Ct

Phase synchronization between objects with periodic behavior emerges in every corner of the natural world, in physical, chemical, biological, and social systems [1]. Although many of the classic examples of synchronization (fireflies, Huygen's clocks, etc.) are macroscopic and classical, synchronization can also be observed in systems where quantum mechanics may lead to inherently nonclassical behavior. Cold atom systems [2–4], nano-mechanical resonators [5–7], spintrolics [8, 9], and frequency combs [10, 11] are a few recent examples of systems that may be useful for gaining basic understanding of how synchronization occurs in the quantum world.

A large amount of recent theoretical work has also been devoted to understanding how quantum mechanics affects various aspects of synchronization [12–18]. In particular, a recent theoretical study [19] has shown that quantum synchronization can occur between two superradiant ensembles of atoms, each emitting ultranarrow laser light into a single optical cavity. The synchronization is manifested as the alignment of the coherent optical dipoles of each ensemble, and at the synchronization point, quantum noise is amplified leading to a large amount of fundamental broadening in the emission spectrum. Here we present a first experimental demonstration of synchronization between two superradiant atomic ensembles. While we do not yet resolve intrinsically quantum behavior, we observe and study key aspects of frequency and phase synchronization between two ensembles of atoms emitting superradiant laser light.

Synchronization is an inherent mechanism in steady state superradiant lasers that allows ultra-narrow linewidth optical lasers (perhaps down to 1 mHz or less) that are highly insensitive to both technical and thermal mirror vibrations [20–23], an optical analog of the microwave hydrogen maser [24]. In such a laser, cavity-mediated interactions combined with repumping-induced dissipation cause the spontaneous synchronization of the phases of the radiating optical dipoles of individual atoms. In the absence of synchronization, the optical dipoles would quickly dephase due to both homogeneous and inhomogeneous broadening, leading to weaker incoherent light emission with a linewidth directly reflecting the width of the broadened atomic transition. Synchronization is thus key to overcoming atomic broadening in order to create narrow optical frequency references that would find a broad range of applications in timekeeping, long-baseline optical interferometry, and precision measurement [25].

In this Letter, we study the synchronization of two distinct sub-ensembles of atoms whose relative optical dipole phases can be externally controlled. We observe several synchronization behaviors. First, we abruptly break the phase alignment between the two collective optical dipoles and observe in real time as synchronization heals the relative phase error, reestablishing laser coherence. Second, we observe steady state synchronization of the two ensembles when a frequency offset is introduced. We confirm synchronization by observing collectively enhanced emission as well as frequency locking of the emitted light.

To form the superradiant laser gain medium, we prepare $N = 1.2 \times 10^6$ ^{87}Rb atoms at 20 μK within a 1D optical lattice in a high-finesse optical cavity with power decay rate $\kappa = 2\pi \times 12$ MHz and single-atom cooperativity $C = 5 \times 10^{-3}$. The lasing transition is a Raman transition from the $|\uparrow\rangle \equiv \left|5^2S_{1/2}, F = 2, m_F = 0\right\rangle$ to $|\downarrow\rangle \equiv \left|5^2S_{1/2}, F = 1, m_F = 0\right\rangle$ ground hyperfine states. In a dressed-state picture, the effective atomic transition frequency is the frequency of the spontaneously emitted Raman photon. The transition frequency is controlled by Raman dressing lasers applied transverse to the cavity axis and tuned 1.3 GHz blue of the $|\uparrow\rangle$ to $|\mathrm{i}\rangle \equiv \left|5^2P_{3/2}, F = 2\right\rangle$ transition. Repumping from $|\downarrow\rangle$ back to $|\uparrow\rangle$ at single-atom rate W is achieved by applying additional lasers transverse to the cavity mode. The repump lasers are not phase matched with the Raman dressing lasers and their spontaneously scattered photons are not resonant with a cavity mode.

To create two spatially separate ensembles with independently controlled optical dipoles, we apply two Raman dressing lasers that address either the upper or lower portions of the total trapped atomic ensemble (Fig. 1). This provides independent control of the dressing laser phases $\alpha_{a,b}$, angular frequencies $\omega_{a,b}$, and intensities as parameterized by a resonant-Rabi flopping angular frequency $\Omega_{a,b}$ for the $|\uparrow\rangle$ to $|\mathrm{i}\rangle$ transition. We can independently set the single-atom Raman decay rates $\gamma_{a,b} (\approx 2\pi \times 250$ Hz) by controlling each laser's inten-

* Corresponding author: keco3197@colorado.edu

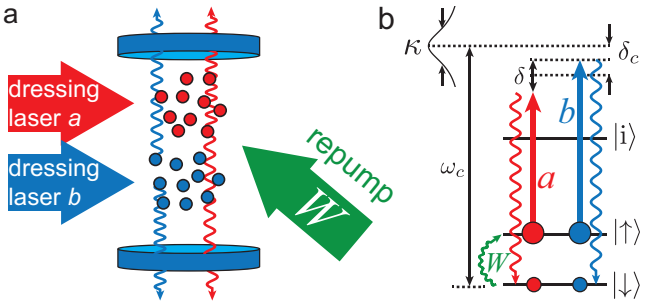

FIG. 1. (Color online) Experimental diagram and Raman lasing energy levels. (a) Two spatially distinct beams (red, blue) dress an ensemble of laser-cooled atoms inside an optical cavity, defining the two superradiant ensembles a and b. Repumping beams (green) are also applied transverse to the cavity. (b) Dressing beams induce Raman decay from $|\uparrow\rangle$ to $|\downarrow\rangle$. Both emitted photon frequencies (wavy lines) are within the linewidth κ of a single cavity mode. The repumping laser returns atoms back to $|\uparrow\rangle$ via single-particle repumping at rate W.

sity. The relative number of atoms $N_{a,b}$ in each ensemble can be controlled by translating the spatial boundary between the dressing lasers along the cavity axis.

Because we utilize Raman transitions for the lasing process, the relevant total optical dipole phases that synchronize are given by $\phi_{a,b} = \eta_{a,b} + \alpha_{a,b}$. Here $\eta_{a,b}$ is the phase associated with the coherence that develops between the ground states $|\uparrow\rangle$ and $|\downarrow\rangle$ in each ensemble. Since the dressing phases are externally controlled parameters, the cavity-mediated interactions drive changes in the ground state coherences $\eta_{a,b}$ to synchronize the optical dipole phases $\phi_{a,b}$.

We first study the dynamics of phase synchronization in the time domain for two ensembles with degenerate frequencies $\delta \equiv \omega_b - \omega_a = 0$. The dressing and repumping lasers are all turned on for 0.1 ms, during which time the two ensembles reach a steady state in which they emit at the same frequency and act as a single synchronized superradiant ensemble with $\phi_a = \phi_b$. An electro-optic crystal is used to quickly jump the phase α_b of the b dressing laser by an amount $\Delta\alpha_b$ in 30 ns. The timescale of the jump is much faster than the time dynamics of the resynchronization process and effectively creates an instantaneous error in the alignment of the optical phases $\phi_b = \phi_a + \Delta\alpha_b$.

To observe how this phase error heals in time, we allow the system to dynamically evolve for a variable amount of time $T_{\text{evol}} = 0$ to 1.5 μs before we rapidly extinguish the other dressing laser, $\Omega_a \to 0$. Subsequently, only ensemble b radiates into the cavity mode. We infer the change in ϕ_b from the difference in the phases $\Delta\psi$ of the emitted light just before the phase jump and just after T_{evol}.

There are several other physical mechanisms that also affect the observed value $\Delta\psi$ that are not directly related to the synchronization between the optical dipoles. The primary contribution to this background phase shift is population inversion-dependent cavity frequency pulling [26]. To remove these less interesting contributions, we measure the light phase difference $\Delta\psi_\pm$ with heterodyne detection for equal magnitude but opposite sign phase jumps $\pm\Delta\alpha_b$. The computed differential quantity $\Delta\bar{\psi} = (\Delta\psi_+ - \Delta\psi_-)/2$ is insensitive to these background systematic errors.

The measured quantity $\Delta\bar{\psi}$ as a function of the evolution time T_{evol} is shown in Fig. 2(b). Here the phase jump is $\Delta\alpha_b = 90°$, and we see that $\Delta\bar{\psi}$ is also 90° near $T_{\text{evol}} = 0$. The phase $\Delta\bar{\psi}$ then relaxes back toward 0°, settling at an intermediate value such that $\phi_a = \phi_b$. A theoretical comparison for the data is derived using an approximate 2-level mean-field model. The model uses independently measured experimental parameters and is described in detail in Ref. [26]. The qualitative behavior and approximate timescales for relaxation are captured by the model.

Since the atomic dipoles resynchronize to the average dipole moment, the equilibrium phase at large T_{evol} is primarily determined by the ratio of the relative magnitudes of the optical dipoles of the two ensembles just before the evolution period. The magnitude of each collective dipole is proportional to the number of participating synchronized atoms ($N_{a,b}$) and the emitted electric field per atom ($\propto \sqrt{\gamma_{a,b}}$). The relative dipole magnitude is then roughly characterized by $R_d \equiv (N_b\sqrt{\gamma_b})/(N_a\sqrt{\gamma_a}) = 1.5$ and 4.0 for the solid and open data sets in Fig. 2(b). Assuming that the total collective dipole phase is constant in time, for $T_{\text{evol}} \gg W^{-1}$ and $\Delta\alpha = 90°$ the measured phase $\Delta\bar{\psi}$ will relax to $\Delta\bar{\psi}_e \equiv \tan^{-1}(R_d)$. The steady state phase given by numerical solutions to the mean-field model is $\Delta\bar{\psi}_n$, with independently measured inputs $N_{a,b}$, $\Omega_{a,b}$, and W.

For the data with more balanced populations (solid), the ensembles equally pull each other's optical phases $\phi_{a,b}$ and the light phase relaxes to $\Delta\bar{\psi} = 51(3)°$, close to $(\Delta\bar{\psi}_e, \Delta\bar{\psi}_n) = (56°, 55°)$. The oscillations that appear in the model depend strongly on the damping rate W. In the more imbalanced (open) data, the unobserved ϕ_a is pulled more rapidly toward the phase of ϕ_b. At the longest T_{evol} in the data, $\Delta\bar{\psi} = 71(2)°$, while $(\Delta\bar{\psi}_e, \Delta\bar{\psi}_n) = (79°, 73°)$, i.e., closer to the phase of ensemble b at $T_{\text{evol}} = 0$.

Synchronization necessarily implies moving from a state of higher entropy to a state of lower entropy, requiring dissipation into a bath of states that absorb the entropy. In our atom-cavity system, one dissipation mechanism for synchronization is the spontaneously scattered optical pumping light involved in re-exciting the atoms from $|\downarrow\rangle$ to $|\uparrow\rangle$ at rate W. Because our atomic ensemble is optically thin in the direction transverse to the laser cavity, the scattering process for the ith atom is not collective and causes single-atom collapse, erasing the relative quantum phase ϕ_i in the single atom superposition state: $\cos(\theta_i/2)\,|\uparrow_i\rangle + e^{\imath\phi_i}\sin(\theta_i/2)\,|\downarrow_i\rangle \to |\uparrow_i\rangle$. It is this relative phase ϕ_i that encodes the phase of the single-atom dipole and thus the phase of the light $\psi_i = \phi_i$ that is radiated by the single oscillator. It is helpful to visualize ϕ_i as the azimuthal phase on the single-dipole Bloch sphere and the angle θ_i as a polar angle. The quantum collapse serves to erase any relative phase error $\Delta\phi_i = \phi_i - \phi_{\text{avg}}$ that had accumulated in time between the individual atom's optical dipole and an appropriately defined average of the phases of all of the optical dipoles of participating atoms ϕ_{avg}.

The total cavity field is the sum of the optical fields radiated

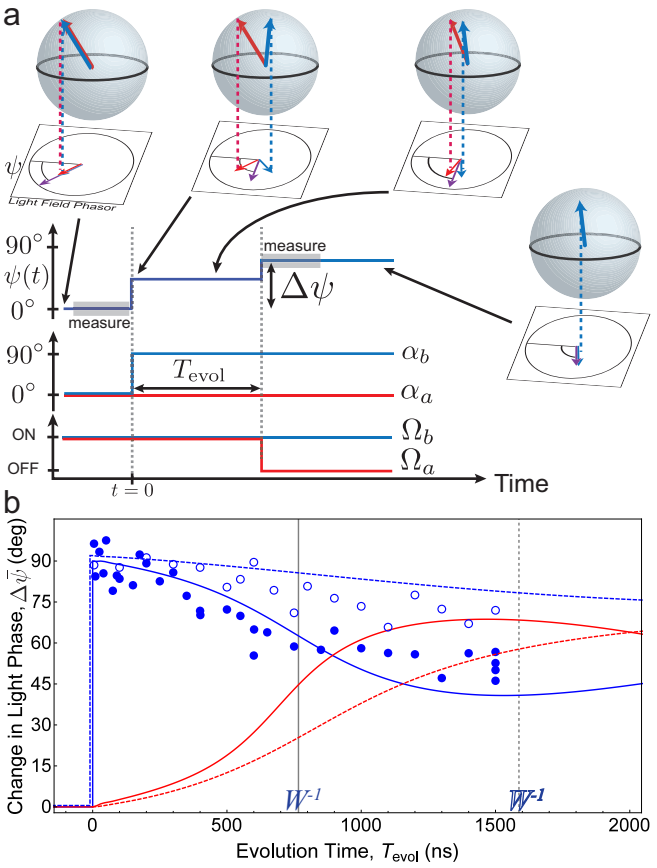

FIG. 2. (Color) Healing of an instantaneous phase error between optical dipoles. (a) Timing diagram and visualization of atomic Bloch vectors. Before time $t = 0$ the two dipoles interact and synchronize. At $t = 0$, dressing laser phase α_b is jumped by 90°. The ensembles' interaction begins to heal the relative phase error. At $t = T_{\text{evol}}$, dressing laser a is turned off ($\Omega_a \to 0$) so that only ensemble b radiates into the cavity. The difference $\Delta\bar{\psi}$ in the phases of the radiated light in the grey windows before $t = 0$ and after $t = T_{\text{evol}}$ indicates the change in the optical dipole phase $\Delta\phi_b = \Delta\bar{\psi}$. The upper panels provide cartoon visualizations of phasors representing the radiated fields (red for a, blue for b, purple for the sum) and Bloch vectors. (b) Light phase change $\Delta\bar{\psi}$ vs. evolution time T_{evol}. The solid and open points correspond to experiments with dipole ratios $R_d = (1.5, 4.0)$ respectively. Vertical solid and dashed lines show the characteristic time scale of the respective single-atom repumping rates for the two data sets $W^{-1} = (0.77, 1.6)$ μs corresponding to (solid, open) data. The solid and dashed curves are the results of a numerical mean-field model for the respective data (red for ensemble a, blue for b).

by each atom, with a resulting phase $\psi_{\text{avg}} = \phi_{\text{avg}}$. This cavity field drives a unitary rotation of a single-atom optical dipole about an axis close to the equatorial plane but not necessarily on the equator due to inhomogeneous broadening, leading to a phase ϕ_i that may not equal ϕ_{avg}. The combination of realignment to the average and subsequent erasure of phase errors through repumping is a useful physical picture for the origin of the quantum synchronization process. This simple model demonstrates why the timescale for synchronization is approximately given by the repumping rate W, and also why the final relaxation phase is approximately $\tan^{-1}(R_d)$.

We observe steady-state synchronization behavior by varying the frequency offset δ between the two ensembles' dressing lasers. When the two ensembles are detuned far away, they emit at their respective atomic transitions, behaving as two independent superradiant lasers in the same cavity mode. However, when the detuning between the ensembles is sufficiently small, the ensembles will phase synchronize and emit as a single laser. For the reasons previously discussed, the detuning δ over which synchronization occurs is set by the repumping rate W. Within a frequency range W we observe signatures of synchronization in both the laser output power and output frequency spectrum.

The phase alignment of the two ensembles is first evident in the output power through the observation of a collective enhancement. Due to constructive interference, the output power is nominally expected to increase by a factor of two when the ensembles synchronize. This observation is presented in Fig. 3. The observed maximum synchronized power output is a factor of $2.2(1)$ greater than the unsynchronized power output. The enhancement is, in fact, expected to deviate slightly from exactly 2.0 due to output power quenching from repumping [21, 27]. Additionally, the slight asymmetry of the total power for positive and negative δ is also reflected in the asymmetric behavior in the spectra of Fig. 4 and discussed below.

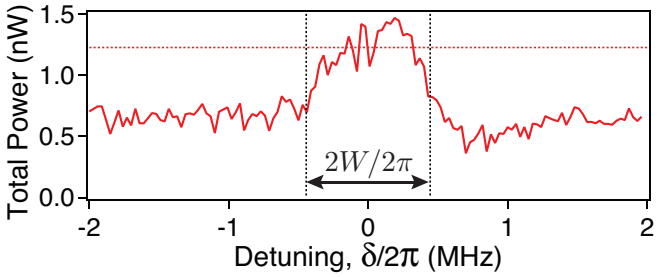

FIG. 3. (Color online) Total power output vs. detuning for the data shown in Fig. 4(a). Vertical dashed lines are at the repumping rate $\pm W/2\pi$. Horizontal dashed line is the predicted maximum synchronized output power.

We can also observe the transition from synchronized to unsynchronized behavior in the laser frequency spectrum by making heterodyne measurements of the light emitted from the cavity. In the spectrograms of Fig. 4, each row is a frequency spectrum of emitted light from the cavity, with brighter colors indicating higher power. Each power spectrum is calculated from 80 μs of the time record. The two-dimensional power spectrum is created by repeating the measurement at a series of different detunings δ, with values shown along the vertical axis.

For $|\delta| \gg W$, the two ensembles of atoms emit at frequencies very close to the unperturbed Raman transition frequencies. As $|\delta|$ decreases, the emission frequencies are pulled toward each other as the rate of relative phase error introduction δ nears the error erasure rate W. We note that we do not observe nor expect a region of repulsive synchronization that appears when injection locking a single superradiant ensemble to an externally applied drive [28], since the effective drive

strength of either of the ensembles on the other does not exceed the detuning δ when $\delta > W$. For $|\delta| \lesssim W$, the erasure of phase errors dominates and the two ensembles radiate at a single frequency.

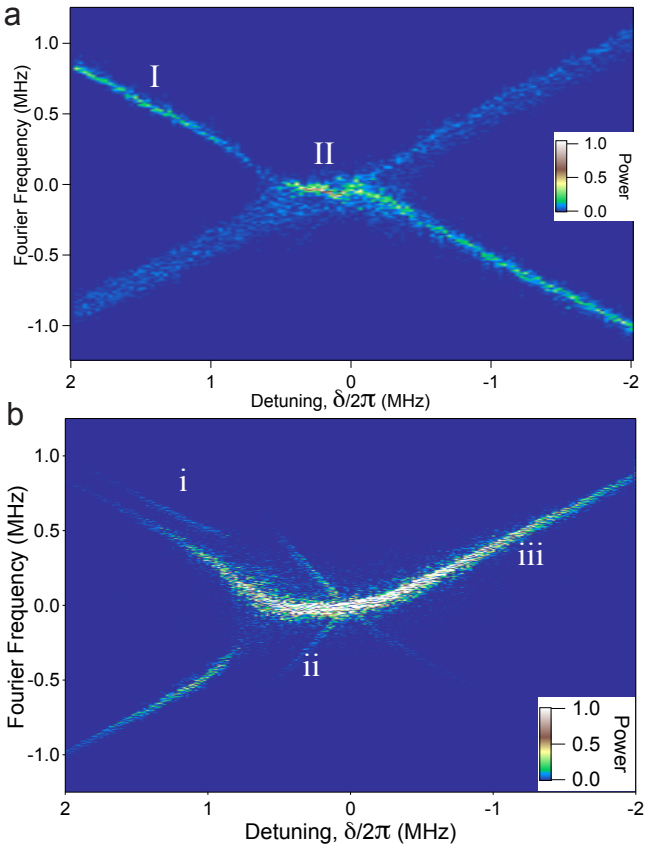

FIG. 4. (Color) Spectrograms of light emitted from two superradiant ensembles. Vertical axis is the Fourier frequency of each power spectrum and horizontal axis is the detuning of dressing lasers δ. The power (color scale) is normalized to the maximum power across the entire spectrogram. (a) Each power spectrum displayed here represents the mean of 5 power spectra at each δ. Collective dipoles are roughly balanced with $N_a/N_b = 0.6$ and $\gamma_a/\gamma_b = 0.8$. (b) Asymmetric operating conditions, $N_a/N_b = 1.1$ and $\gamma_a/\gamma_b = 1.6$.

The observed spectrum qualitatively agrees with the mean-field expectation [19], exhibiting a hyperbolic-like approach (Region I) to the synchronized state (Region II). However, there is significant asymmetry in the power spectrum. Part of this asymmetry arises from a finite detuning of the average Raman transition frequency from resonance with the cavity resonance frequency by amount $\delta_c = -2\pi \times 4$ MHz $\approx \kappa/3$, an operating condition favorable for suppressing relaxation oscillations [26, 29] yet one that introduces an imbalance in the coupling to the cavity between ensembles. Other causes of asymmetry are imbalances in the optical dipole magnitudes (both N and γ) for the data in Fig. 4. Numerical modeling indicates that the effects of these small asymmetries are magnified by the interaction between the ensembles.

We also show in Fig. 4(b) that distinct qualitative behaviors can be observed depending on the operating parameters. This data shows a significant asymmetry in the emitted power (iii) from each ensemble for $\delta > 0$ and $\delta < 0$. Many of these behaviors are observed in numerical mean-field models of our system, but other features, indicated in Fig. 4(b) are not: (i) the parallel-running frequency component in the lower right hand quadrant, (ii) the extra frequency components at $\pm\delta/2\pi$, and the asymmetry in the observed linewidth of the two emission peaks of both Fig. 4(a) and (b). The fractional power in each sideband (ii) is small, $< 8\%$ of the total power in each spectrum.

In prior studies, linewidth broadening was seen to arise from an inversion-dependent frequency-pulling mechanism that here would cause a common broadening of both peaks [21, 26]. Attempts to identify other classical mechanisms for the asymmetric broadening (e.g., fluctuating AC Stark shifts or interference between dressing beams) have been unsuccessful and the broadening phenomenon remains an interesting topic for future theoretical and experimental study, with the intriguing possibility that this is a fundamental quantum noise effect [19].

Overall, the three observations of this paper clearly demonstrate the key elements of synchronization in the gain medium of a superradiant laser, offering a unique ability to observe the establishment of coherence in the laser (Fig. 1). We believe these observations are a first step toward understanding what role intrinsically quantum effects play in the synchronization process. Moreover, some of the unexplained behavior, particularly unexplained broadening in Fig. 4, may hint at the quantum noise amplification predicted by Ref. 19. However, significant further study will be required to identify intrinsically quantum behavior.

In addition to future fundamental studies of quantum synchronization, we expect this work to be useful for future technologically relevant implementations of superradiant ensembles that would produce optically narrow light [20, 21]. For instance, two ensembles that utilize atomic transitions with opposite sensitivity to magnetic fields could use synchronization to cancel magnetic field noise, without alternating measurements as is done in passive optical lattice clocks [30]. Also, this work points toward a coupled atom-cavity system for exploring quantum noise in phase transition models [19], using atomic synchronization for enhanced Ramsey spectroscopy [31], and overcoming the Dick effect by transferring coherence between atomic clocks [32, 33].

ACKNOWLEDGMENTS

The authors acknowledge early contributions by Matthew A. Norcia. All authors acknowledge financial support from DARPA QuASAR, ARO, NSF PFC, and NIST. K.C.C. acknowledges support from NDSEG. This work is supported by the National Science Foundation under Grant Number 1125844.

[1] S. Strogatz, *Sync: The emerging science of spontaneous order* (Hyperion, 2003).

[2] F. Brennecke, R. Mottl, K. Baumann, R. Landig, T. Donner, and T. Esslinger, Proceedings of the National Academy of Sciences **110**, 11763 (2013).

[3] J. Klinder, H. Keßler, M. Wolke, L. Mathey, and A. Hemmerich, Proceedings of the National Academy of Sciences **112**, 3290 (2015).

[4] C. Hamner, C. Qu, Y. Zhang, J. Chang, M. Gong, C. Zhang, and P. Engels, Nature communications **5** (2014).

[5] M. Zhang, G. S. Wiederhecker, S. Manipatruni, A. Barnard, P. McEuen, and M. Lipson, Phys. Rev. Lett. **109**, 233906 (2012).

[6] M. Bagheri, M. Poot, L. Fan, F. Marquardt, and H. X. Tang, Phys. Rev. Lett. **111**, 213902 (2013).

[7] M. H. Matheny, M. Grau, L. G. Villanueva, R. B. Karabalin, M. C. Cross, and M. L. Roukes, Phys. Rev. Lett. **112**, 014101 (2014).

[8] S. Kaka, M. R. Pufall, W. H. Rippard, T. J. Silva, S. E. Russek, and J. A. Katine, Nature **437**, 389 (2005).

[9] S. Sani, J. Persson, S. Mohseni, Y. Pogoryelov, P. Muduli, A. Eklund, G. Malm, M. Käll, A. Dmitriev, and J. Åkerman, Nat Commun **4**, (2013).

[10] Y. H. Wen, M. R. E. Lamont, A. L. Gaeta, I. M. Kloumann, and S. H. Strogatz, arXiv (2014), arXiv:1412.0119v1.

[11] P. Del'Haye, K. Beha, S. B. Papp, and S. A. Diddams, Phys. Rev. Lett. **112**, 043905 (2014).

[12] A. Mari, A. Farace, N. Didier, V. Giovannetti, and R. Fazio, Phys. Rev. Lett. **111**, 103605 (2013).

[13] O. V. Zhirov and D. L. Shepelyansky, Phys. Rev. B **80**, 014519 (2009).

[14] T. E. Lee, C.-K. Chan, and S. Wang, Phys. Rev. E **89**, 022913 (2014).

[15] T. E. Lee and H. R. Sadeghpour, Phys. Rev. Lett. **111**, 234101 (2013).

[16] S. Walter, A. Nunnenkamp, and C. Bruder, Phys. Rev. Lett. **112**, 094102 (2014).

[17] I. Hermoso de Mendoza, L. A. Pachón, J. Gómez-Gardeñes, and D. Zueco, Phys. Rev. E **90**, 052904 (2014).

[18] D. Jaksch, S. A. Gardiner, K. Schulze, J. I. Cirac, and P. Zoller, Phys. Rev. Lett. **86**, 4733 (2001).

[19] M. Xu, D. A. Tieri, E. C. Fine, J. K. Thompson, and M. J. Holland, Phys. Rev. Lett. **113**, 154101 (2014).

[20] D. Meiser, J. Ye, D. R. Carlson, and M. J. Holland, Phys. Rev. Lett. **102**, 163601 (2009).

[21] J. G. Bohnet, Z. Chen, J. M. Weiner, D. Meiser, M. J. Holland, and J. K. Thompson, Nature **484**, 78 (2012).

[22] M. A. Norcia and J. K. Thompson, Physical Review X **6**, 011025 (2016).

[23] M. A. Norcia, M. N. Winchester, J. R. K. Cline, and J. K. Thompson, Science Advances **2** (2016), 10.1126/sciadv.1601231.

[24] D. Kleppner, H. M. Goldenberg, and N. F. Ramsey, Phys. Rev. **126**, 603 (1962).

[25] T. Kessler, C. Hagemann, C. Grebing, T. Legero, U. Sterr, F. Riehle, M. J. Martin, L. Chen, and J. Ye, Nature Photonics **6**, 687 (2012), 1112.3854.

[26] J. G. Bohnet, Z. Chen, J. M. Weiner, K. C. Cox, and J. K. Thompson, Phys. Rev. A **89**, 013806 (2014).

[27] D. Meiser and M. J. Holland, Phys. Rev. A **81**, 033847 (2010).

[28] K. C. Cox, J. M. Weiner, and J. K. Thompson, Phys. Rev. A **90**, 053845 (2014).

[29] J. G. Bohnet, Z. Chen, J. M. Weiner, K. C. Cox, and J. K. Thompson, Phys. Rev. Lett. **109**, 253602 (2012).

[30] B. J. Bloom, T. L. Nicholson, J. R. Williams, S. L. Campbell, M. Bishof, X. Zhang, W. Zhang, S. L. Bromley, and J. Ye, Nature **506**, 71 (2014).

[31] M. Xu and M. J. Holland, (2014), arXiv:1407.5132.

[32] T. Rosenband and D. R. Leibrandt, arXiv (2013), arXiv:1303.6357v2.

[33] J. Borregaard and A. S. Sørensen, Phys. Rev. Lett. **111**, 090802 (2013).